Volume 13
Number 16
28 April 2022
Pages 4427–4656

Chemical Science

rsc.li/chemical-science

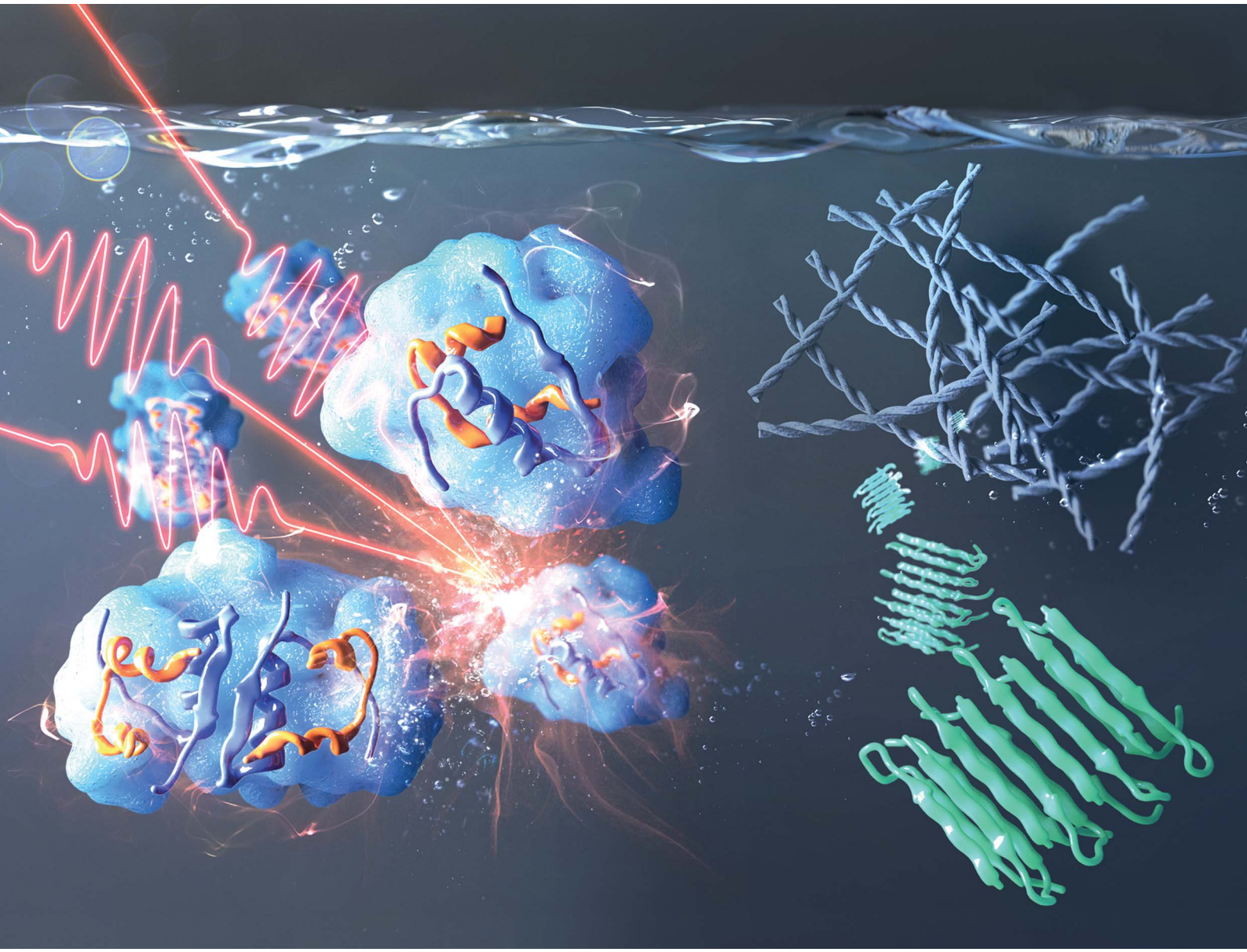

ISSN 2041-6539

ROYAL SOCIETY OF CHEMISTRY

EDGE ARTICLE

Hugh I. Kim, Kyungwon Kwak, Minhaeng Cho *et al.*
Direct observation of protein structural transitions through entire amyloid aggregation processes in water using 2D-IR spectroscopy

Chemical Science

ROYAL SOCIETY OF CHEMISTRY

EDGE ARTICLE

View Article Online
View Journal | View Issue

Cite this: *Chem. Sci.*, 2022, **13**, 4482

All publication charges for this article have been paid for by the Royal Society of Chemistry

Direct observation of protein structural transitions through entire amyloid aggregation processes in water using 2D-IR spectroscopy†

So Yeon Chun,‡[ab] Myung Kook Son,‡[bcd] Chae Ri Park,[bcd] Chaiho Lim,[ab] Hugh I. Kim,*[bcd] Kyungwon Kwak*[ab] and Minhaeng Cho*[ab]

Amyloid proteins that undergo self-assembly to form insoluble fibrillar aggregates have attracted much attention due to their role in biological and pathological significance in amyloidosis. This study aims to understand the amyloid aggregation dynamics of insulin (INS) in H_2O using two-dimensional infrared (2D-IR) spectroscopy. Conventional IR studies have been performed in D_2O to avoid spectral congestion despite distinct H–D isotope effects. We observed a slowdown of the INS fibrillation process in D_2O compared to that in H_2O. The 2D-IR results reveal that different quaternary structures of INS at the onset of the nucleation phase caused the distinct fibrillation pathways of INS in H_2O and D_2O. A few different biophysical analysis, including solution-phase small-angle X-ray scattering combined with molecular dynamics simulations and other spectroscopic techniques, support our 2D-IR investigation results, providing insight into mechanistic details of distinct structural transition dynamics of INS in water. We found the delayed structural transition in D_2O is due to the kinetic isotope effect at an early stage of fibrillation of INS in D_2O, *i.e.*, enhanced dimer formation of INS in D_2O. Our 2D-IR and biophysical analysis provide insight into mechanistic details of structural transition dynamics of INS in water. This study demonstrates an innovative 2D-IR approach for studying protein dynamics in H_2O, which will open the way for observing protein dynamics under biological conditions without IR spectroscopic interference by water vibrations.

Received 2nd November 2021
Accepted 18th March 2022

DOI: 10.1039/d1sc06047c

rsc.li/chemical-science

Introduction

Amyloid proteins undergo self-assembly to form insoluble fibrillar aggregates with a common architecture of unbranched, highly ordered β-sheets. For many amyloid proteins, fibrils and intermediates such as oligomers are associated with various human diseases, known as amyloidosis.[2,3] The complex fibrillation process of amyloid aggregation is affected by diverse biological factors, as it involves dynamic structural heterogeneity and diverging mechanisms, making it challenging to understand and control. Therefore, much effort has been undertaken to understand the structural details of the oligomeric species at an early stage of the fibrillation process at the molecular level.[4–9] Among various amyloid proteins, insulin (INS), a critical hormone that regulates glucose homeostasis, is associated with injection localized amyloidosis in type II diabetes.[10] INS is prone to form amyloid fibers under various pH, concentration, salt, buffering agent, and temperature conditions.[11] INS is also known to form polymorphic amyloid fibrils depending on aggregation conditions.[12,13] Therefore, understanding the mechanisms of INS fibrillation in various experimental conditions is necessary for developing therapeutic strategies for amyloidosis.

To study amyloid-associated protein dynamics, tremendous efforts have been made to track the appropriate structural dynamics of the intermediates generated in the aggregation processes by using spectroscopic techniques such as X-ray crystallography and nuclear magnetic resonance (NMR) spectroscopy,[14–16] which monitor protein structural dynamics on timescales from nanoseconds to years. In particular, protein dynamics on subnanosecond timescales can be studied by infrared (IR) spectroscopy, utilizing nine characteristic IR absorption bands inherent in proteins, specifically amide A, B, and I–VII. Among these, the spectral lineshape and frequency of the amide I band, primarily the C=O stretch vibrations of the peptide linkages, are exceptionally sensitive to secondary structural elements of a protein. Therefore, time-resolved amide I IR spectroscopy with high temporal resolution (<ps) is one of

[a]*Center for Molecular Spectroscopy and Dynamics, Institute for Basic Science (IBS), Seoul 02841, Republic of Korea. E-mail: kkwak@korea.ac.kr; mcho@korea.ac.kr*
[b]*Department of Chemistry, Korea University, Seoul 02841, Republic of Korea. E-mail: hughkim@korea.ac.kr*
[c]*Center for Proteogenome Research, Korea University, Seoul 02841, Republic of Korea*
[d]*Single Cell Analysis Laboratory, Korea University, Seoul 02841, Republic of Korea*

† Electronic supplementary information (ESI) available: Details of experimental methods and supplementary results. See DOI: 10.1039/d1sc06047c

‡ These authors contributed equally to this work.

the most incisive tools for studying protein dynamics in condensed phases. Despite these advantages, the spectral overlap between the H–O–H bending mode of H_2O (δ_{H-O-H}, 1650 cm^{-1}) and the amide I mode ($\nu_{C=O}$, 1600–1700 cm^{-1}) prohibits the direct application of various IR spectroscopic techniques to the studies of proteins dissolved in ordinary water. Most IR studies have thus been performed in D_2O to avoid spectral congestion, and they have been undoubtedly successful in determining and monitoring protein structure and dynamics.[17,18] In addition, solution NMR, one of the most extensively used methods in protein dynamics studies, typically uses 10% D_2O to stabilize the magnetic field strength and lock the field-dependent frequency. However, nuclear quantum effects[19–21] arising from tunneling, nuclear delocalization, zero-point energy differences, and other H–D isotope effects[22] could, in general, influence the properties of proteins.[23,24] For example, it was reported that the stability of folded proteins in D_2O differs from that in H_2O, leading to different aggregation rates,[22,23,25–27] especially in the fibrillation of amyloid proteins since water plays a key role in modulating the transition free energy of amyloid nucleation.[28–30] Furthermore, the use of D_2O could result in substantial changes in the couplings between heavy water and protein vibrations due to the frequency shifts of water bending and stretching modes upon H–D exchange,[31,32] which would alter the energy transfer and vibrational relaxation processes. Therefore, the IR spectroscopy of a protein in heavy water could differ from that in ordinary water, implying that an extra layer of caution is necessary when generalizing the IR spectroscopic results on protein folding–unfolding or aggregation processes in D_2O.

Over the past two decades, two-dimensional IR (2D-IR) spectroscopy, an IR analog of 2D-NMR, has become a powerful tool for studying protein dynamics.[17,33] In a 2D-IR spectrum, off-diagonal peaks produced by vibrational couplings provide information about the spatial and chemical connectivity between two oscillators. Furthermore, the real-time monitoring of 2D-IR diagonal and off-diagonal peaks and their lineshapes enables the rates of conformational transitions, vibrational relaxation, and local solvent fluctuations. In addition, the nonlinear dependence of the 2D-IR signal on oscillator strengths makes the contrast between strongly and weakly IR-absorbing modes more prominent than those of linear IR spectroscopy, often resulting in an enhanced spectral resolution.[18,34–36] Because of these advantages of 2D-IR technique with an improved spectral resolution, it was used to identify intermediates during amyloid protein aggregation processes and track the mechanism of amyloid fibril formation at the molecular level.[37,38] More importantly, the improved temporal resolution enables the selective gating of slowly decaying signals in the time domain. For example, the vibrational lifetime of the protein amide I mode, which is in the range from 0.5 to 1 ps depending on secondary structures and the extent of solvent exposure,[32,39–41] is substantially longer than that of the δ_{H-O-H} of H_2O (~170 fs). As a consequence, there is the Goldilocks time window during which the protein 2D-IR signal remains strong without interfering with water contributions, which allows one to measure the 2D-IR spectra of proteins selectively even in H_2O.

In this work, we investigated the distinct amyloid fibrillation processes of human INS in H_2O and D_2O using 2D-IR spectroscopy. In addition to addressing fundamental questions regarding the isotope effects of D_2O on protein dynamics, we aim to understand the causes of the different amyloid aggregation kinetics of INS in H_2O and D_2O. We observed a slowdown of the fibrillation process of INS in D_2O compared to that in H_2O. Here, we show that this difference in INS fibrillations originates from the distinctively different tertiary structures of INS in H_2O and D_2O. Various ancillary spectroscopic and biophysical techniques allowed us to gain further insights into the details of the

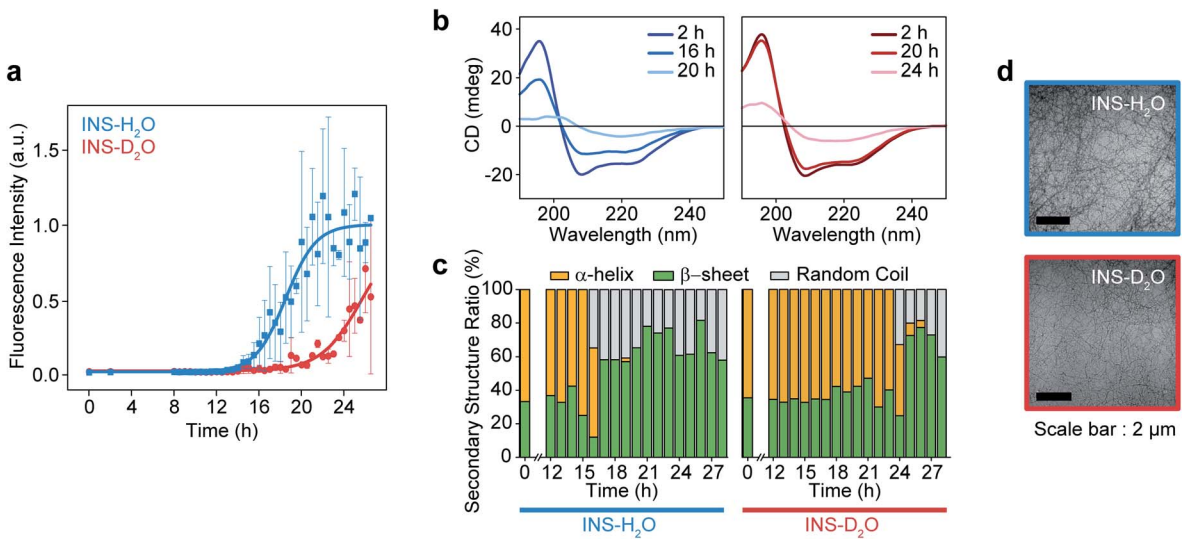

Fig. 1 Fibrillation process kinetic analysis of INS in H_2O and D_2O at 17 mg mL^{-1} concentration. (a) The plot of ThT fluorescence spectra at the intensity of 490 nm. (b) CD spectra of INS in H_2O and D_2O during fibrillation. (c) The ratio of secondary structures (β-sheet, α-helix, and random coil) from analysis of CD spectrum using BeStSel server.[1] (d) TEM image after the fibrillation process (~28 h) of INS-H_2O (top) and INS-D_2O (bottom).

structural transitions during the initial stage, nucleation and lag phase, and fibril elongation process of INS in water.

Results and discussion

Kinetics of insulin fibrillation

The fibrillation kinetics of INS (17 mg mL^{-1}) in H_2O and D_2O were examined using the standard thioflavin T (ThT) fluorescence assay method (Fig. 1a). The stiff rise of ThT fluorescence intensity is an indication of the formation of fibrils. Interestingly, under our experimental conditions (INS-H_2O at pH = 2.1, INS-D_2O at pD = 2.1, 50 °C, and 25 rpm for incubation), the fibrillation (~16 h) of INS in H_2O occurs earlier than that (~20 h) in D_2O (ESI Note I). This observation was further confirmed by the measured circular dichroism (CD) spectra, which exhibited a slightly faster conversion of α-helix-rich INS into β-sheet fibrils in H_2O than in D_2O (Fig. 1b, c, S1, Tables S1 and S2†).[42] However, no significant difference in fibril morphology was observed in TEM images of INS fibrils formed in H_2O and D_2O (Fig. 1d). We observed that the fibrillations of INS in H_2O occur faster than those in D_2O at different experimentally measured pH (pH^M) values (HCl (DCl)–KCl buffer solution, pH^M = 1.7, 2.1, and 2.5).

To understand this result, we noted that D_2O molecules could form a stronger deuterium bond (D-bond) between D_2O molecules, which induces a greater number of D-bonds per molecule than H-bonds per H_2O in water.[22,23] Thus, the entropic cost of dissolving a solute molecule in D_2O is, in general, higher than that in H_2O. Accordingly, D_2O effectively increases the hydrophobic interactions between amino acid residues in INS, thereby increasing the thermodynamic stability (ΔG_u, free energy of unfolding) and enthalpy of unfolding (ΔH_u) of INS.[24,26] The helical propensity of INS in D_2O lasts longer than that in H_2O, which was observed in the time-resolved CD spectra and supports this supposition (Tables S1, S2 and Fig. S5†).[25,26]

Linear IR and 2D-IR spectroscopy of insulin fibrillation

To investigate the distinct structural dynamics of INS, which induce different fibrillation kinetics in H_2O and D_2O, we examined the amide I IR absorption spectra of INS after subtracting the solvent spectrum from the raw spectrum (ESI Note II†). For the INS-water solution, such solvent background correction should be performed carefully because the H_2O bending signal substantially overlaps with the amide I band of INS and because the two vibrations could mix *via* H-bonding interactions. When INS is dissolved in D_2O, the H–D exchange processes of the peptide N–H groups should be completed before the IR measurements (ESI Note III). The different fibrillation rates in H_2O and D_2O observed in the ThT fluorescence assay and CD spectroscopy could also be confirmed using linear IR spectroscopy. The time-resolved IR spectra of INS (Fig. 2a) suggest that the conformational transition from an α-helix-rich structure

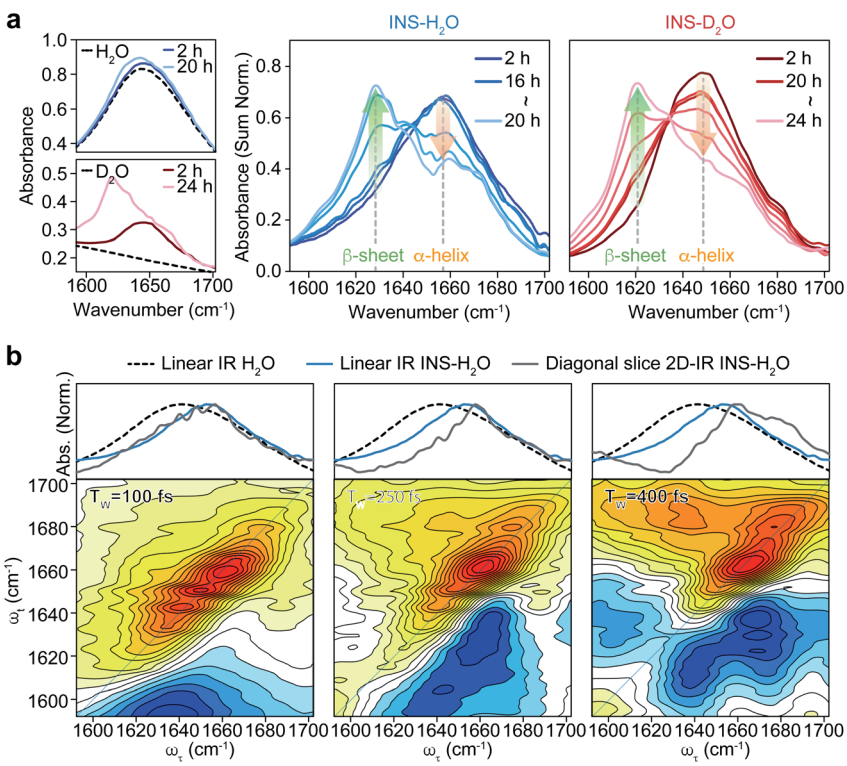

Fig. 2 Linear IR of INS during fibrillation and waiting time (T_W) dependent 2D-IR spectra of INS. (a) Area-normalized linear IR absorption spectra of INS in H_2O and D_2O obtained during incubation. The raw linear IR spectra of two solvents (H_2O and D_2O) and INS-solvent, showing the signal overlap of H–O–H bending mode of water and protein amide I band at 1650 cm^{-1}, are shown in the left. (b) Spectra comparison of linear IR spectra of H_2O, INS-H_2O, and diagonal slice 2D-IR spectra of INS-H_2O (top) and 2D-IR spectra of INS-H_2O at a waiting time of 100, 250, and 400 fs (bottom).

(~1658 cm^{-1} in H_2O and ~1649 cm^{-1} in D_2O) to a β-sheet-rich fibrillar structure (~1629 cm^{-1} in H_2O and ~1620 cm^{-1} in D_2O) occurs faster in H_2O than in D_2O.[43–45]

We next carried out 2D-IR measurements of INS sampled intermittently from the incubation vessel (Fig. 2b, ESI Note IV†). It is known that the molar absorption coefficient of the amide I vibration is larger than that of H_2O.[46,47] Therefore, 2D-IR spectroscopy, whose signal is proportional to the fourth power of the vibrational transition dipole moment, is quite useful for distinguishing the strong amide I mode of INS from the H_2O signal.[48,49] However, the 2D-IR spectra at waiting times (T_w) shorter than 200 fs are still governed by the signal from H_2O. Other undesired pump-induced heating signals contributed to the 2D-IR spectra after 300 fs.[39] Because the lifetime of δ_{H-O-H} of H_2O (~170 fs) is much shorter than that of the amide I vibration (0.5–1 ps), the H_2O signal rapidly decreases as the pump-probe delay time T_w increases. From these experimental observations, the ideal range of T_w for selective 2D-IR measurements of protein amide I modes is from 200 to 300 fs (Fig. 2b).[50]

The 2D-IR diagonal slice spectra at T_w = 250 fs reveal the distinctive difference in INS structures (Fig. 3). The dominant features in the 2D-IR spectra of INS in H_2O and D_2O in the early stage of incubation (~2 h) are the broad peaks at 1660 cm^{-1} and 1651 cm^{-1}, respectively, which correspond to the α-helix in native INS. The characteristic features of the β-sheets appear in the INS-H_2O 2D-IR spectrum at ~1627 cm^{-1} only after 16 h of incubation. However, D_2O delays the conversion of INS from an α-helix to a β-sheet. More specifically, the 2D-IR peak associated with the β-sheets at ~1616 cm^{-1} becomes noticeable after 20 h of incubation. Surprisingly, the 2D-IR diagonal slice spectra at an early stage of INS fibrillation in H_2O and D_2O differ from each other, suggesting distinctly different initial structures. In H_2O, the broad featureless peak at 1660 cm^{-1} is due to the α-helix (Fig. 3a). The spectrum in D_2O exhibits additional $\nu_\perp$ (~1642 cm^{-1}) and $\nu_\parallel$ (~1680 cm^{-1}) peaks that reflect the presence of β-strands in addition to the α-helix (Fig. 3b and S13†).[51] These 2D-IR results strongly suggest that INS proteins tend to form dimers in D_2O with antiparallel β-sheets.[52–54]

After the fibrillation process was completed, we confirmed the antiparallel β-sheet structures of INS fibrils in H_2O and D_2O using the 2D-IR technique; we used the main diagonal β-sheet peaks at 1627 and 1616 cm^{-1}, respectively, weak high-frequency diagonal peaks at approximately 1673 and 1665 cm^{-1}, respectively, and the cross-peaks (Fig. S14†).[51,55,56] Thus, despite the different structures of INS in the early stages of fibrillation, we

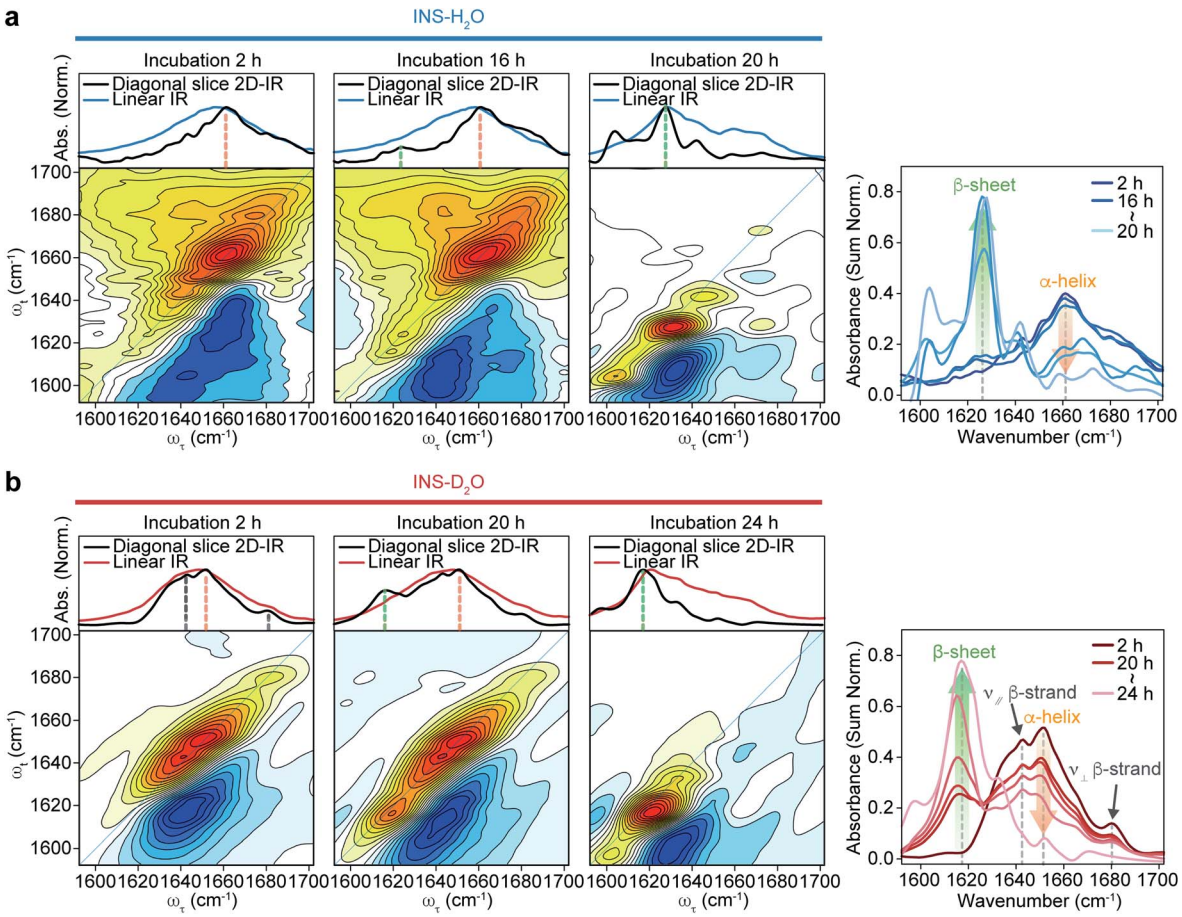

Fig. 3 2D-IR spectra of INS during fibrillation. Spectra comparison of linear IR spectra and diagonal slice 2D-IR spectra (top) and 2D-IR spectra (bottom) of INS-H_2O (a) and INS-D_2O (b) obtained during incubation at a waiting time of 250 fs. The diagonal slice 2D-IR spectra of INS-H_2O and INS-D_2O obtained during incubation at a waiting time of 250 fs are shown in the right (INS-H_2O: 2, 16–20 h, INS-D_2O: 2, 20–24 h, 1 h interval).

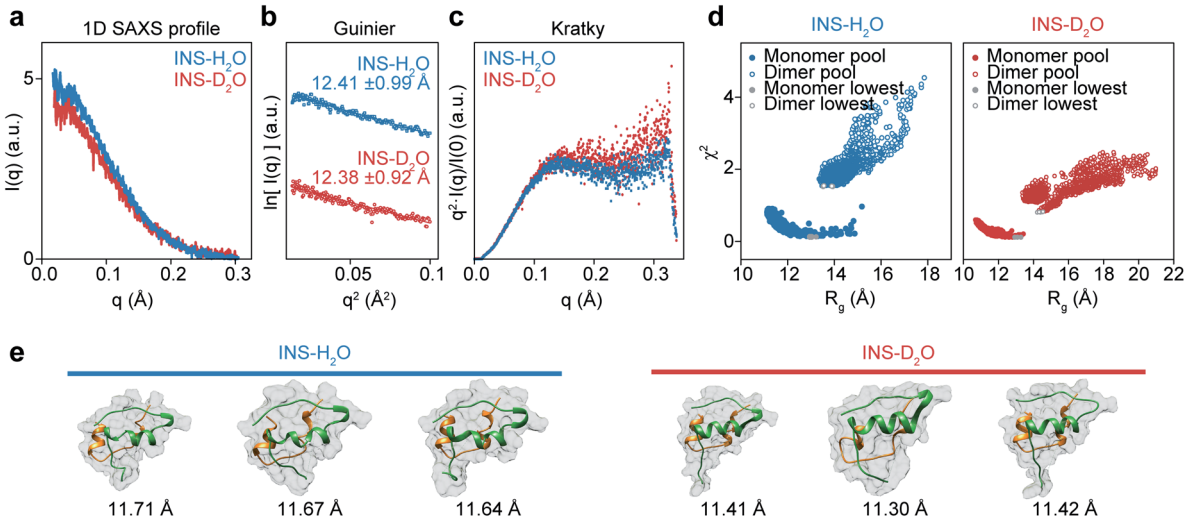

Fig. 4 Solution phase SAXS analysis of INS (INS-H_2O (blue), INS-D_2O (red)) and theoretical structures of INS obtained with MD-simulation. (a) Experimental SAXS scattering profiles of INS 2 mg mL^{-1} in pH (pD) = 2.1. (b) Guinier plot obtained from short q range of scattering profile. (c) Normalized Kratky analysis of INS. (d) χ^2–R_g diagram of INS-H_2O and INS-D_2O from the MD-simulated 22 000 conformations, obtained with CRYSOL. Filled colored circles at the bottom left are the 14 000 monomer conformations and filled red circles are the candidate structures of INS monomers with the smallest χ^2 values. Empty colored circles at the top right are the 8000 dimer conformations and empty red circles are the INS dimers with the smallest χ^2 values. (e) Candidate structures of INS-H_2O and INS-D_2O obtained with CRYSOL of MD-simulated monomer, dimer structure pools. 3 structures with the smallest χ^2 structures were used as candidate structures.

found no significant difference in the final fibril structures even with 2D-IR spectroscopy.

From these experimental findings, we believe that the distinct initial structures of INS in H_2O and D_2O induce the difference in nucleation kinetics. INS proteins are known to exist in complex forms under physiological conditions. Therefore, the dissociation of dimers into monomers is required for nucleation and subsequent prefibril formation, followed by amyloid fibrillation under acidic conditions. Thus, the presence of INS dimers in D_2O could be a factor delaying the initial nucleation step and the overall fibrillation process.

Structural dynamics of INS in the early stages of amyloid fibrillation

Although it is plausible that the enhanced hydrophobic interactions in D_2O could stabilize the intermolecular β-sheet structure in the INS dimer,[57,58] it is necessary to investigate the initial structures of INS at a low concentration of 2 mg mL^{-1} (25 °C) to estimate the average sizes using solution-phase small-angle X-ray scattering (SAXS). The 1D SAXS profiles of INS in H_2O and D_2O are shown in Fig. 4a. The radii of gyration (R_g) obtained from the Guinier analysis of $I(q)$ are 12.41 ± 0.99 Å and 12.38 ± 0.92 Å for INS in H_2O and D_2O, respectively (Fig. 4b). Kratky analysis of the SAXS profiles (Fig. 4c), which provide information about the flexibility and structural disorder of a given protein, suggest that INS in H_2O and D_2O adopt similar globular conformations.[59] The observations that the experimentally determined R_g values of INS are slightly larger than that of the INS monomer (Fig. S15,† ~11.6 Å from the 3E7Y PDB structure)[12] and that the R_g of INS in H_2O is slightly larger than that in D_2O indicate the presence of mixed forms of INS with complex structures.

Then, we studied the structures of INS by carrying out MD simulations. Noting that the SAXS results show the presence of a heterogeneous structural mixture of INS, we performed simulated annealing MD simulations to generate 14 000 monomeric and 8000 dimeric structures. Then, the representative candidate structures were selected by comparing them with experimental scattering profiles (Fig. 4d).[60] We found that the fraction of INS dimers in D_2O was approximately 10%, whereas it was nearly zero in H_2O (Table 1). Additionally, the simulated candidate structures of monomeric INS exhibited an enhanced helical propensity in D_2O compared to those in H_2O (Fig. 4e and Table 2). The dimers in D_2O formed intermolecular β-sheet structures, which is consistent with our 2D-IR results. At a low INS concentration of 2 mg mL^{-1} in the SAXS measurements, a relatively small fraction of the proteins could form dimers, while increased dimer formation was expected at the

Table 1 Monomer/dimer ratio of MD-simulated candidate structures calculated using OLIGOMER. The smaller the χ^2 is, the more accurate the experimental and MD-simulated data matches

	χ^2	Monomer fraction	Dimer fraction
INS-H_2O	0.54	100.0% (±7.9%)	0
	0.56	100.0% (±0.4%)	0
	0.68	86.6% (±1.5%)	13.4% (±1.1%)
	0.69	90.5% (±1.6%)	9.5% (±1.1%)
	0.71	89.1% (±1.6%)	10.9% (±1.1%)
INS-D_2O	0.49	93.4% (±1.9%)	6.6% (±1.5%)
	0.5	88.9% (±2.3%)	11.1% (±1.6%)
	0.5	92.4% (±1.9%)	7.6% (±1.5%)
	0.51	90.6% (±2.1%)	9.4% (±1.6%)
	0.54	98.0% (±106.9%)	2.0% (±2.4%)

Table 2 R_g and helicity of INS monomer (3E7Y PDB structure, Fig. S15, ESI) and candidate structures of INS-H_2O and INS-D_2O (Fig. 5)

		H_2O				D_2O			
	INS monomer	Exp. avg	MD-1	MD-2	MD-3	Exp. avg	MD-1	MD-2	MD-3
R_g (Å)	11.6	12.41	11.71	11.67	11.64	12.38	11.41	11.30	11.42
Helicity (%)	56	—	37.3	29.4	43.1	—	43.1	43.1	49.0

high concentration of 17 mg mL^{-1} used in the 2D-IR experiments. As discussed earlier, the fibrillation of INS is still faster in H_2O than D_2O even at low concentrations (1 and 2 mg mL^{-1}) of the protein (ESI Note I†), indicating that the difference in the fibrillation mechanisms of INS in two water solvents revealed by the 2D-IR spectroscopy remains valid even for comparatively low protein concentration solutions.

Kinetic control in INS fibril assembly by H_2O and D_2O

Many protein assemblies *in vivo* are diffusion-controlled reactions, where the transport rate of the protein (*i.e.*, the diffusion coefficient of the protein) is critical for determining the reaction rate.[61–63] As D_2O is more viscous than H_2O, the INS diffusion coefficient (D_{INS}) is smaller in D_2O than in H_2O. Thus, we also considered the potential effects of the distinct viscosities of H_2O and D_2O on the fibrillation kinetics of INS (ESI Note V†). The fibrillation processes of INS (1 mg mL^{-1}) in H_2O and D_2O were examined after the protein was fully denatured (*i.e.*, monomeric highly disordered state, Fig. S17†) using sodium dodecyl sulfate (SDS 50 μM, 50 °C, 75 rpm) to confirm the effect of denaturation on protein fibrillation.

Interestingly, we found that the fibrillation of INS was no longer significantly more accelerated in H_2O than in D_2O when the initial INS proteins were in a fully denatured state before incubation (Fig. S18†). This result indicates that the fibrillation kinetics of INS are dominantly affected by the unfolding transition of the INS monomer or dimer under our experimental conditions (H_2O at pH = 2.1, D_2O at pD = 2.1, 50 °C, 1–17 mg mL^{-1} INS) rather than by viscosity-dependent diffusion processes. In addition, time-resolved monitoring of INS fibrillation with FT-IR further supports our supposition that the initial denaturation process, which is independent of protein–protein collision, is the critical step during INS fibrillation (Fig. S19†).

Then, we measured the stability of INS before fibril formation using differential scanning calorimetry (DSC) (Fig. S20† and Table 3).[64] The thermal transition temperature (T_0), enthalpy (ΔH_u), and entropy (ΔS_u) upon INS unfolding in H_2O were 59.55 °C, 42.53 kJ mol^{-1}, and 128.3 J K^{-1}, respectively. The T_0 of INS in D_2O (61.83 °C) was slightly higher than that of H_2O,

Table 3 Thermodynamic analysis of INS unfolding based on DSC thermograms

	T_0 (°C)	ΔH_u (kJ mol^{-1})	ΔS_u (J mol^{-1} K^{-1})
INS-H_2O	59.55	42.53	128.3
INS-D_2O	61.38	46.99	140.8

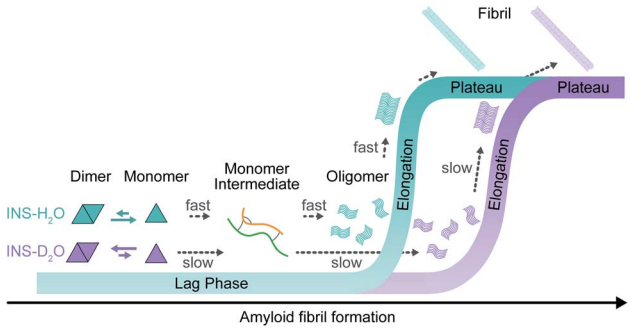

Fig. 5 Fibrillation kinetics diagram of INS, based on kinetic and structural analysis. INS-H_2O (blue) and INS-D_2O (purple).

which implies that the protein was stabilized by enhanced hydrophobic interactions and dimer formation. The INS exhibited a slightly larger ΔH_u (46.99 kJ mol^{-1}) and ΔS_u (140.8 J K^{-1}) in D_2O than in H_2O, indicating the increased thermal stability and the propensity of INS dimer formation in heavy water. This result also confirms that the dissociation of the dimer to monomers followed by the formation of a partially unfolded INS intermediate in D_2O requires a higher free energy cost than that in H_2O. Based on the nucleation-growth mechanism, the formed nuclei interact with partially unfolded monomers to elongate and form prefibrils. This delayed formation of partially denatured monomeric intermediates further delays the elongation process of INS fibrillation in D_2O, which is consistent with the 2D-IR observation that the slow fibrillation of INS in D_2O results from the dissociation of INS dimers followed by the delayed denaturation of each INS monomer in D_2O.

Conclusions

We investigated the effects of deuterated aqueous environments on the protein dynamics associated with amyloid fibrillation of INS. The fibrillation process occurs slowly in D_2O compared with that in H_2O. Using the advantage of 2D-IR, the amide I band of INS, which is a diagnostic signature of protein secondary structure, can be measured in H_2O without spectral congestion and interference by water bending vibrations. The ability to suppress the water background signal using time-selective 2D-IR spectroscopy enabled investigations into different structures of INS that were hard to resolve by other spectroscopic measurements (*e.g.*, ThT fluorescence, CD, and IR spectroscopy). Dimer formation of INS in D_2O induces a delayed structural transition required for the

subsequent protein nucleation process at an early stage of fibrillation (Fig. 5). The SAXS, MD, and DSC results provide additional insight into mechanistic details of the protein structural transitions involved in each fibrillation step. Unexpectedly, we found substantial kinetic isotope effects on the amyloid fibrillation of INS. This result highlights the importance of using H_2O instead of D_2O in various time-resolved IR spectroscopic studies of protein dynamics. We anticipate that the present work will shed light on the mechanism of amyloidosis under physiological conditions through the use of nonlinear IR microspectroscopy with improved spatial and temporal resolution.

Author contributions

MC, KK, and HIK designed the experiments; SYC, MKS, CRP, and CL carried out various experiments; SYC, MKS, HIK, and KK analyzed experimental data; SYC, MKS, HIK, KK, and MC wrote the manuscript with input from all the authors.

Conflicts of interest

There are no conflicts to declare.

Acknowledgements

This research was supported by a grant from the Institute for Basic Science (IBS-R023-D1) and by the National Research Foundation of Korea (NRF) grant funded by the Korean government (MSIT) (NRF-2020R1A5A1019141). This research was also supported by the Korea Basic Science Institute (KBSI) National Research Facilities & Equipment Center (NFEC), funded by the Korean government (Ministry of Education) (2019R1A6C1010028). This work was also supported by Basic Research Program No. 2019R1H1A2079867 and No. 2019R1A2C2086193 through the National Research Foundation (NRF) of Korea, funded by the Ministry of Science, ICT, and Future Planning (MSIP). This work was also supported by the National Research Foundation of Korea (NRF) grant funded by the Korean government (MSIT) (2021R1A4A1032114). The synchrotron X-ray scattering measurements at the 4C SAXS II beamline of the Pohang Accelerator Laboratory were supported by the Ministry of Education and Science Technology. The authors thank the National Center for Seoul National University Research Facilities for their assistance with the TEM measurements.

Notes and references

1 A. Micsonai, F. Wien, É. Bulyáki, J. Kun, É. Moussong, Y.-H. Lee, Y. Goto, M. Réfrégiers and J. Kardos, *Nucleic Acids Res.*, 2018, **46**, W315–W322.
2 M. Goedert and M. G. Spillantini, *Science*, 2006, **314**, 777–781.
3 P. J. McLean, H. Kawamata and B. T. Hyman, *Neuroscience*, 2001, **104**, 901–912.
4 E. E. Cawood, T. K. Karamanos, A. J. Wilson and S. E. Radford, *Biophys. Chem.*, 2021, **268**, 106505.
5 B. R. Sahoo, S. J. Cox and A. Ramamoorthy, *Chem. Commun.*, 2020, **56**, 4627–4639.
6 M. I. Ivanova, Y. Lin, Y.-H. Lee, J. Zheng and A. Ramamoorthy, *Biophys. Chem.*, 2021, **269**, 106507.
7 S. A. Kotler, J. R. Brender, S. Vivekanandan, Y. Suzuki, K. Yamamoto, M. Monette, J. Krishnamoorthy, P. Walsh, M. Cauble, M. M. B. Holl, E. N. G. Marsh and A. Ramamoorthy, *Sci. Rep.*, 2015, **5**, 11811.
8 G. J. Morgan, *Biophys. Chem.*, 2022, **281**, 106711.
9 D. Milardi, E. Gazit, S. E. Radford, Y. Xu, R. U. Gallardo, A. Caflisch, G. T. Westermark, P. Westermark, C. L. Rosa and A. Ramamoorthy, *Chem. Rev.*, 2021, **121**, 1845–1893.
10 A. Ahmad, V. N. Uversky, D. Hong and A. L. Fink, *J. Biol. Chem.*, 2005, **280**, 42669–42675.
11 L. Nielsen, R. Khurana, A. Coats, S. Frokjaer, J. Brange, S. Vyas, V. N. Uversky and A. L. Fink, *Biochemistry*, 2001, **40**, 6036–6046.
12 T. S. Choi, J. W. Lee, K. S. Jin and H. I. Kim, *Biophys. J.*, 2014, **107**, 1939–1949.
13 D. Bernson, A. Mecinovic, M. T. Abed, F. Lime, P. Jageland, M. Palmlof and E. K. Esbjorner, *Eur. Biophys. J.*, 2020, **49**, 145–153.
14 J. Chugh, S. Sharma and R. V. Hosur, *Protein Sci.*, 2008, **17**, 1319–1325.
15 I. R. Kleckner and M. P. Foster, *Biochim. Biophys. Acta*, 2011, **1814**, 942–968.
16 R. B. Fenwick, H. van den Bedem, J. S. Fraser and P. E. Wright, *Proc. Natl. Acad. Sci. U. S. A.*, 2014, **111**, E445–E454.
17 P. Hamm and M. Zanni, *Concepts and Methods of 2D Infrared Spectroscopy*, Cambridge University Press, 2011.
18 Z. Ganim, H. S. Chung, A. W. Smith, L. P. DeFlores, K. C. Jones and A. Tokmakoff, *Acc. Chem. Res.*, 2008, **41**, 432–441.
19 A. Berger, G. Ciardi, D. Sidler, P. Hamm and A. Shalit, *Proc. Natl. Acad. Sci. U. S. A.*, 2019, **116**, 2458–2463.
20 B. R. Shrestha, S. Pillai, A. Santana, S. H. Donaldson Jr, T. A. Pascal and H. Mishra, *J. Phys. Chem. Lett.*, 2019, **10**, 5530–5535.
21 J. Guo, X.-Z. Li, J. Peng, E.-G. Wang and Y. Jiang, *Prog. Surf. Sci.*, 2017, **92**, 203–239.
22 Y. Marcus and A. Ben-Naim, *J. Chem. Phys.*, 1985, **83**, 4744–4759.
23 G. C. Kresheck, H. Schneider and H. A. Scheraga, *J. Phys. Chem.*, 1965, **69**, 3132–3144.
24 S. S. Stadmiller and G. J. Pielak, *Protein Sci.*, 2018, **27**, 1710–1716.
25 S.-Y. Sheu, E. W. Schlag, H. Selzle and D.-Y. Yang, *J. Phys. Chem. A*, 2008, **112**, 797–802.
26 B. W. Chellgren and T. P. Creamer, *J. Am. Chem. Soc.*, 2004, **126**, 14734–14735.
27 M. Reslan and V. Kayser, *Pharm. Dev. Technol.*, 2018, **23**, 1030–1036.
28 L. Jean, C. F. Lee, P. Hodder, N. Hawkins and D. J. Vaux, *Sci. Rep.*, 2016, **6**, 32124.

29 J. Roche, Y. Shen, J. H. Lee, J. Ying and A. Bax, *Biochemistry*, 2016, **55**, 762–775.
30 A. D. Stephens, J. Kölbel, R. Moons, M. T. Ruggerio, N. Mahmoudi, T. A. Shmool, T. M. McCoy, D. Nietlispach, A. F. Routh, F. Sobott, J. A. Zeitler and G. S. K. Schierle, *bioRxiv*, 2021.
31 D. Czurlok, J. Gleim, J. Lindner and P. Vöhringer, *J. Phys. Chem. Lett.*, 2014, **5**, 3373–3379.
32 J. Tan, J. Zhang, C. Li, Y. Luo and S. Ye, *Nat. Commun.*, 2019, **10**, 1–6.
33 M. Cho, *Two-Dimensional Optical Spectroscopy*, CRC press, 2009.
34 N. Demirdöven, C. M. Cheatum, H. S. Chung, M. Khalil, J. Knoester and A. Tokmakoff, *J. Am. Chem. Soc.*, 2004, **126**, 7981–7990.
35 L. P. DeFlores, Z. Ganim, R. A. Nicodemus and A. Tokmakoff, *J. Am. Chem. Soc.*, 2009, **131**, 3385–3391.
36 A. M. Woys, A. M. Almeida, L. Wang, C.-C. Chiu, M. McGovern, J. J. De Pablo, J. L. Skinner, S. H. Gellman and M. T. Zanni, *J. Am. Chem. Soc.*, 2012, **134**, 19118–19128.
37 Y. L. Ling, D. B. Strasfeld, S.-H. Shim, D. P. Raleigh and M. T. Zanni, *J. Phys. Chem. B*, 2009, **113**, 2498–2505.
38 L. E. Buchanan, E. B. Dunkelberger, H. Q. Tran, P. N. Cheng, C. C. Chiu, P. Cao, D. P. Raleigh, J. J. De Pablo, J. S. Nowick and M. T. Zanni, *Proc. Natl. Acad. Sci. U. S. A.*, 2013, **110**, 19285–19290.
39 S. Hume, G. M. Greetham, P. M. Donaldson, M. Towrie, A. W. Parker, M. J. Baker and N. T. Hunt, *Anal. Chem.*, 2020, **92**, 3463–3469.
40 S. Hume, G. Hithell, G. M. Greetham, P. M. Donaldson, M. Towrie, A. W. Parker, M. J. Baker and N. T. Hunt, *Chem. Sci.*, 2019, **10**, 6448–6456.
41 C. T. Middleton, L. E. Buchanan, E. B. Dunkelberger and M. T. Zanni, *J. Phys. Chem. Lett.*, 2011, **2**, 2357–2361.
42 N. J. Greenfield, *Nat. Protoc.*, 2006, **1**, 2876–2890.
43 L. N. Garriques, S. Frokjaer, J. F. Carpenter and J. Brange, *J. Pharm. Sci.*, 2002, **91**, 2473–2480.
44 M. Bouchard, J. Zurdo, E. J. Nettleton, C. M. Dobson and C. V. Robinson, *Protein Sci.*, 2000, **9**, 1960–1967.
45 F. Piccirilli, S. Mangialardo, P. Postorino, L. Baldassarre, S. Lupi and A. Perucchi, *Soft Matter*, 2012, **8**, 11863–11870.
46 A. A. Laogun, R. J. Sheppard and E. H. Grant, *Phys. Med. Biol.*, 1984, **29**, 519–524.
47 S. Y. Venyaminov and F. G. Prendergast, *Anal. Biochem.*, 1997, **248**, 234–245.
48 N. T. Hunt, *Chem. Soc. Rev.*, 2009, **38**, 1837–1848.
49 C. N. Pace, F. Vajdos, L. Fee, G. Grimsley and T. Gray, *Protein Sci.*, 1995, **4**, 2411–2423.
50 N. Huse, S. Ashihara, E. T. J. Nibbering and T. Elsaesser, *Chem. Phys. Lett.*, 2005, **404**, 389–393.
51 A. W. Smith and A. Tokmakoff, *J. Chem. Phys.*, 2007, **126**, 045109.
52 Z. Ganim, K. C. Jones and A. Tokmakoff, *Phys. Chem. Chem. Phys.*, 2010, **12**, 3579–3588.
53 W. G. Turnell and J. T. Finch, *J. Mol. Biol.*, 1992, **227**, 1205–1223.
54 C. F. Hjorth, M. Norrman, P.-O. Wahlund, A. J. Benie, B. O. Petersen, C. M. Jessen, T. Å. Pedersen, K. Vestergaard, D. B. Steensgaard, J. S. Pedersen, H. Naver, F. Hubálek, C. Poulsen and D. Otzen, *J. Pharm. Sci.*, 2016, **105**, 1376–1386.
55 S. Hahn, S.-S. Kim, C. Lee and M. Cho, *J. Chem. Phys.*, 2005, **123**, 084905.
56 S. J. Roeters, A. Iyer, G. Pletikapić, V. Kogan, V. Subramaniam and S. Woutersen, *Sci. Rep.*, 2017, **7**, 41051.
57 V. N. Uversky, L. N. Garriques, I. S. Millett, S. Frokjaer, J. Brange, S. Doniach and A. L. Fink, *J. Pharm. Sci.*, 2003, **92**, 847–858.
58 Y. Pocker and S. B. Biswas, *Biochemistry*, 1981, **20**, 4354–4361.
59 C. D. Putnam, M. Hammel, G. L. Hura and J. A. Tainer, *Q. Rev. Biophys.*, 2007, **40**, 191–285.
60 D. Svergun, C. Barberato and M. H. J. Koch, *J. Appl. Crystallogr.*, 1995, **28**, 768–773.
61 M. Oliveberg and P. G. Wolynes, *Q. Rev. Biophys.*, 2005, **38**, 245–288.
62 M. Schlosshauer and D. Baker, *Protein Sci.*, 2004, **13**, 1660–1669.
63 P. E. Schavemaker, A. J. Boersma and B. Poolman, *Front. Mol. Biosci.*, 2018, **5**, 93.
64 L. Liu, C. Yang and Q.-X. Guo, *Biophys. Chem.*, 2000, **84**, 239–251.